

Optical conductivity of bismuth-based topological insulators

P. Di Pietro,¹ F. M. Vitucci,¹ D. Nicoletti,² L. Baldassarre,³ P. Calvani,¹ R. Cava,⁴ Y. S. Hor,⁴ U. Schade,⁵ and S. Lupi⁶

¹CNR-SPIN and Dipartimento di Fisica, Università di Roma “La Sapienza,” Piazzale A. Moro 2, Roma I-00185, Italy

²Max Planck Research Department for Structural Dynamics, Center for Free Electron Laser Science, University of Hamburg, Notkestrasse 85, Hamburg 22607, Germany

³Sincrotrone Trieste, Area Science Park, Trieste I-34012, Italy

⁴Department of Chemistry, Princeton University, New Jersey 08544, USA

⁵Berliner Elektronenspeicherring-Gesellschaft für Synchrotronstrahlung m.b.H., Albert-Einstein Strasse 15, Berlin, D-12489 Germany

⁶CNR-IOM and Dipartimento di Fisica, Università di Roma “La Sapienza,” Piazzale A. Moro 2, Roma I-00185, Italy

(Received 24 January 2012; revised manuscript received 18 May 2012; published 24 July 2012)

The optical conductivity $\sigma_1(\omega)$ and the spectral weight SW of four topological insulators with increasing chemical compensation (Bi_2Se_3 , $\text{Bi}_2\text{Se}_2\text{Te}$, $\text{Bi}_{2-x}\text{Ca}_x\text{Se}_3$, and $\text{Bi}_2\text{Te}_2\text{Se}$) have been measured from 5 to 300 K and from subterahertz to visible frequencies. The effect of compensation is clearly observed in the infrared spectra through the suppression of an extrinsic Drude term and the appearance of strong absorption peaks that we assign to electronic transitions among localized states. From the far-infrared spectral weight SW of the most compensated sample ($\text{Bi}_2\text{Te}_2\text{Se}$), one can estimate a density of charge carriers on the order of $10^{17}/\text{cm}^3$ in good agreement with transport data. Those results demonstrate that the low-energy electrodynamics in single crystals of topological insulators, even at the highest degree of compensation presently achieved, is still influenced by three-dimensional charge excitations.

DOI: 10.1103/PhysRevB.86.045439

PACS number(s): 78.30.-j, 71.55.-i, 73.25.+i, 78.20.Ci

I. INTRODUCTION

Topological insulators (TIs) are new quantum materials with an insulating gap in the bulk, of spin-orbit origin, and metallic states at the surface.¹⁻³ These states are chiral and show transport properties protected from backscattering by the time-reversal symmetry. In addition to their fundamental properties, such as exotic superconductivity^{4,5} and axionic electromagnetic response,^{6,7} TIs have potential applications in quantum computing,^{8,9} terahertz (THz) detectors,¹⁰ and spintronic devices.¹¹ After the discovery of a topological behavior in three-dimensional (3D) $\text{Bi}_x\text{Sb}_{1-x}$,¹² Bi_2Se_3 recently emerged, thanks to its large bulk insulating gap ($E_G \sim 300$ meV) as the best candidate for the study of topological surface states.¹³ In fact, Dirac quasiparticles (DQPs) related to the topological surface states have been detected through angle-resolved photoemission spectroscopy in Bi_2Se_3 , Bi_2Te_3 , and in their alloys $\text{Bi}_2\text{Se}_2\text{Te}$ and $\text{Bi}_2\text{Te}_2\text{Se}$.^{12,14} Investigating the charge transport and cyclotron resonances of DQPs has, however, proven to be challenging because the surface current contribution is usually obscured by the extrinsic bulk carriers response.¹⁵⁻¹⁷

Indeed, as-grown crystals of Bi_2Se_3 display a finite density of Se vacancies, which act as electron donors. They pin the bulk chemical potential μ_b within the conduction band, thus, producing, over a wide range of carrier concentrations, extrinsic n -type degenerate semiconducting behavior. Se vacancies also affect the low-energy transport properties of those materials,¹⁸ making it difficult to distinguish the intrinsic metallic behavior due to the topological surface state from the extrinsic metallic conduction induced by the Se non-stoichiometry. As a consequence, both transport and optical conductivity experiments^{16,19} show a metallic behavior with a Drude term confined at low frequencies ($\omega < 600$ cm^{-1}), which mirrors the extrinsic carrier content. Two phonon peaks, interacting with the electronic continuum, have been observed in the far-infrared (FIR) range near 61 cm^{-1} (α mode) and

133 cm^{-1} (β mode).^{16,20} The bulk insulating gap instead spans between 250 and 350 meV, depending on the Se vacancy content, in good agreement with theoretical calculations.²¹ At variance with Bi_2Se_3 , single crystals of Bi_2Te_3 display p -type conductivity related to an excess of Bi atoms acting as acceptor centers.¹⁵ These shift μ_b into the valence band so that, such as for Bi_2Se_3 , an extrinsic Drude term is observed in the FIR (here, below $\omega < 400$ cm^{-1}).²²

Motivated by the above observations, different authors adopted specific strategies to reduce the non-stoichiometry-induced bulk carriers in Bi_2Se_3 (Bi_2Te_3) materials. Hor *et al.* showed that Ca doping in the Bi site ($\text{Bi}_{2-x}\text{Ca}_x\text{Se}_3$) progressively shifts μ_b from the conduction band to the valence band, thus, changing as-grown n -type Bi_2Se_3 into a p -type degenerate semiconductor.¹⁸ By exploiting the different doping chemistries of Bi_2Se_3 (n type) and Bi_2Te_3 (p type), a better compensation was obtained in the $\text{Bi}_2\text{Se}_2\text{Te}$ and $\text{Bi}_2\text{Te}_2\text{Se}$ alloys.^{23,24} In both systems, a high resistivity at low T (exceeding 1 Ω cm) was observed at low T . Moreover, in $\text{Bi}_2\text{Se}_2\text{Te}$, the variable range-hopping behavior expected for an impurity-driven conductivity was found²³ to give place, below 20 K, to a T independent σ_{dc} . This crossover was reported as providing evidence that surface conductance prevails at low T in the best compensated system.²³

However, as far as we know, the effects of chemical compensation have not been investigated on the optical properties of those materials. In this paper, we fill this gap, by presenting optical data for four topological insulators— $\text{Bi}_{2-x}\text{Ca}_x\text{Se}_3$ ($x = 0, 0.0002$), $\text{Bi}_2\text{Se}_2\text{Te}$, and $\text{Bi}_2\text{Te}_2\text{Se}$ —from 5 to 300 K and from the sub-THz to the visible spectral range. The effects of the enhanced compensation are clearly visible in the FIR spectra through the suppression of the Drude term and the appearance of strong absorption peaks that we assign to electronic transitions among localized states, similar to those found in weakly doped semiconductors. Our

data show that the electrodynamics of $\text{Bi}_2\text{Te}_2\text{Se}$, i.e., the most compensated sample, is still affected by 3D doped charges as therein, the FIR spectral weight is higher than the spectral weight associated with topological states by nearly 2 orders of magnitude.

II. EXPERIMENT

Single crystals with $x = 0$ were grown by a modified Bridgeman method, and those of $\text{Bi}_{2-x}\text{Ca}_x\text{Se}_3$ were grown via a process of two-step melting.¹⁸ Chemical compensation (i.e., the insulating character) increases when passing from Bi_2Se_3 and $\text{Bi}_2\text{Se}_2\text{Te}$ to $\text{Bi}_{2-x}\text{Ca}_x\text{Se}_3$ and $\text{Bi}_2\text{Te}_2\text{Se}$.²⁴ The basal (ab)-plane resistivity $\rho_{ab}(T)$ of the most compensated sample, $\text{Bi}_2\text{Te}_2\text{Se}$, shows an increasing (semiconducting) behavior down to about 50 K followed by a low- T regime in which resistivity saturates at values exceeding $1 \Omega \text{ cm}$. In this regime, surface charge-carrier mobility, much higher than the bulk mobility, has been experimentally detected.^{24,25}

The reflectivity $R(\omega)$ of the four single crystals was measured at near-normal incidence with respect to the ab basal plane from sub-THz to visible frequencies at temperatures ranging from 5 to 300 K, shortly after cleaving the sample. The reference was obtained by *in situ* evaporation of gold (silver) in the infrared (visible) range. In the sub-THz region (below 30 cm^{-1}), we used the coherent synchrotron radiation extracted from the electron storage ring BESSY II when working in the so-called *low- α* mode.²⁶ The real part of the optical conductivity $\sigma_1(\omega)$ was obtained from $R(\omega)$ via Kramers-Kronig transformations after extrapolating $R(\omega)$ to zero frequency by Drude-Lorentz (D-L) fits. The extrapolations for high frequency were based on data from Ref. 27.

III. RESULTS AND DISCUSSION

The reflectivity data for all samples are shown in Fig. 1. The FIR spectra in Figs. 1(a) and 1(b) are dominated by a free-carrier plasma edge around 500 cm^{-1} , which confirms the picture of an extrinsic electrodynamics in these materials. In $\text{Bi}_{1.9998}\text{Ca}_{0.0002}\text{Se}_3$ [Fig. 1(c)], Ca doping shifts the plasma edge to about 400 cm^{-1} , whereas, the strongest compensation is achieved in $\text{Bi}_2\text{Te}_2\text{Se}$ [Fig. 1(d)] where unshielded phonons are well resolved at 60 (α mode) and 130 (β mode) cm^{-1} . In all spectra, a strong electronic absorption appears above $10\,000 \text{ cm}^{-1}$.

The real part of the optical conductivity obtained from the $R(\omega)$ in Fig. 1 by Kramers-Kronig transformations is shown for the same temperatures and frequencies in Fig. 2. The direct-gap transition, which corresponds to a small bump around 3000 cm^{-1} , is barely visible due to its superposition with the huge triplet electronic excitation present above $10\,000 \text{ cm}^{-1}$. These interband features, which are not the focus of this paper, have been discussed in detail in Ref. 27. Most of the effects induced by compensation appear below 500 cm^{-1} . In particular, the most extrinsic system, Bi_2Se_3 [Fig. 2(a)], presents a Drude term superimposed to the α - and β -phonon peaks, which both sharpen for decreasing T . A similar behavior has been observed in Ref. 16 on a crystal with a comparable charge-carrier density ($\sim 10^{18}/\text{cm}^3$, see below). The effect of compensation becomes observable in $\text{Bi}_2\text{Se}_2\text{Te}$ [Fig. 2(b)]. Here, at variance with an appreciable

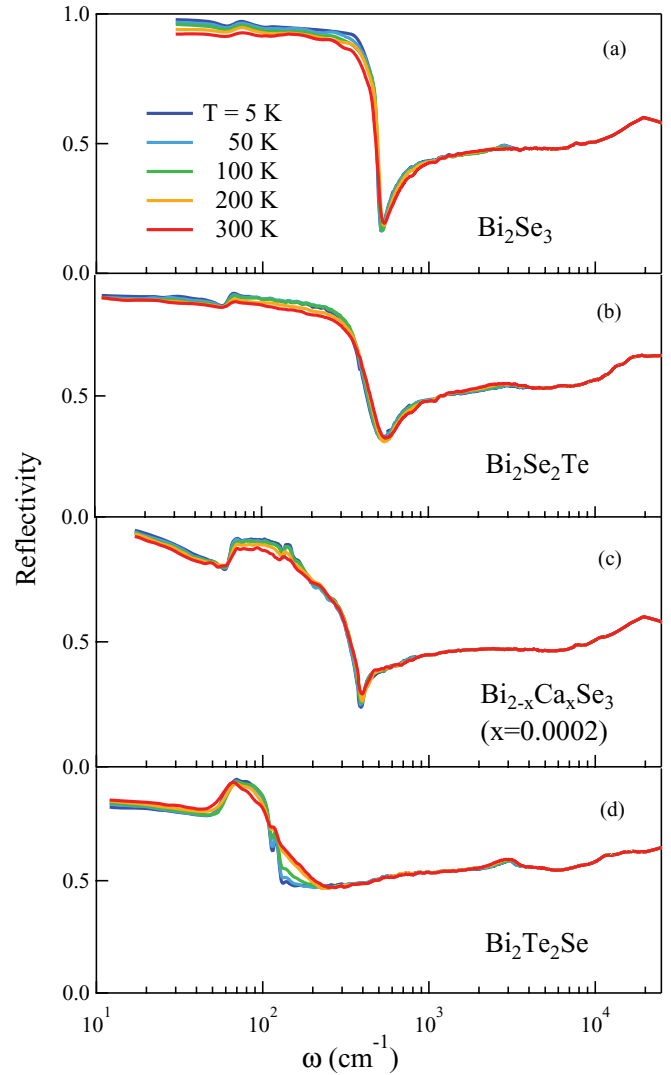


FIG. 1. (Color online) Reflectivity of (a) Bi_2Se_3 , (b) $\text{Bi}_2\text{Se}_2\text{Te}$, (c) $\text{Bi}_{1.9998}\text{Ca}_{0.0002}\text{Se}_3$, and (d) $\text{Bi}_2\text{Te}_2\text{Se}$ from 10 to $24\,000 \text{ cm}^{-1}$ at different temperatures. The FIR spectra in (a)–(c) are characterized by a free-carrier plasma edge around 500 cm^{-1} (400 cm^{-1}) as well as phonon features α and β at about 60 and 130 cm^{-1} , respectively. In (d), due to a strong compensation (see text), the phonon absorptions can be clearly observed. In all spectra, a weak bump develops at low T around 3000 cm^{-1} , corresponding to the direct-gap transition. The triplet direct gap appears instead above $10\,000 \text{ cm}^{-1}$.

dc conductivity ($\sigma_{dc} \sim 200 \Omega^{-1} \text{ cm}^{-1}$,²⁸) most of the FIR spectral weight is located at finite frequencies in the phonon spectral region. A further drastic reduction in the spectral weight is finally obtained in $\text{Bi}_{1.9998}\text{Ca}_{0.0002}\text{Se}_3$ and $\text{Bi}_2\text{Se}_2\text{Te}$ [Figs. 2(c) and 2(d)].

The α -phonon mode, in both $\text{Bi}_2\text{Se}_2\text{Te}$ and $\text{Bi}_{1.9998}\text{Ca}_{0.0002}\text{Se}_3$, shows a Fano line shape with a low-frequency dip, more pronounced at low temperatures. This suggests an interaction of this mode with an electronic continuum at lower frequencies.²⁹ The Fano shape is much less evident in $\text{Bi}_2\text{Te}_2\text{Se}$ where the α phonon shows a nearly Lorentzian shape at room temperature and a weak low-frequency dip at low T . This indicates a transfer of the electronic continuum SW from above to below the phonon

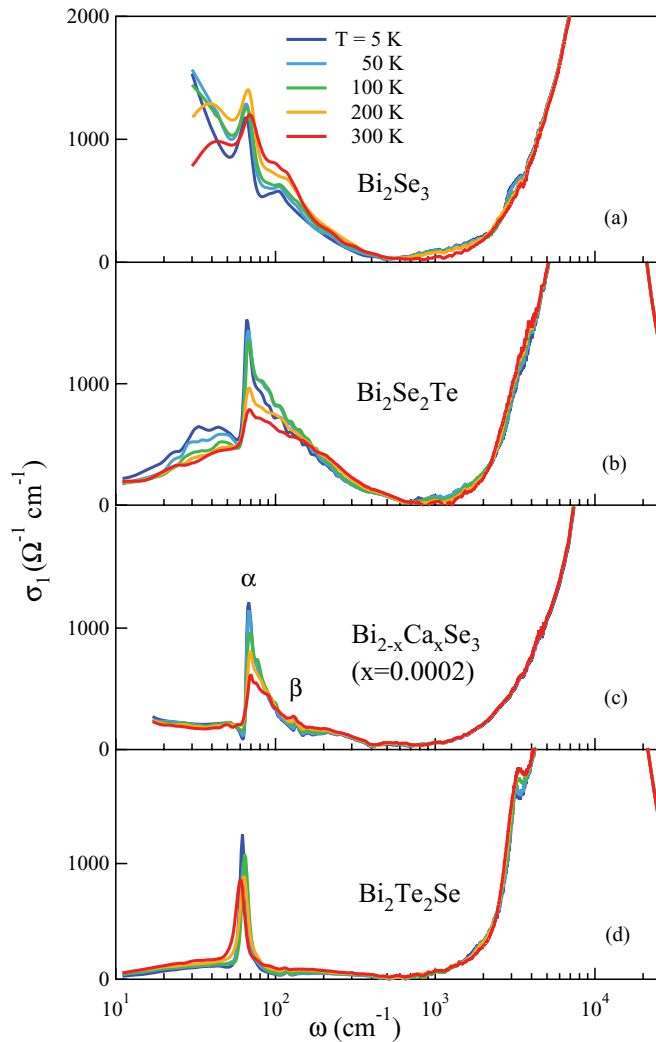


FIG. 2. (Color online) Real part of the optical conductivity of (a) Bi_2Se_3 , (b) $\text{Bi}_2\text{Se}_2\text{Te}$, (c) $\text{Bi}_{1.9998}\text{Ca}_{0.0002}\text{Se}_3$, and (d) $\text{Bi}_2\text{Te}_2\text{Se}$ from 10 to 24 000 cm^{-1} at different temperatures. A broad minimum around 500 cm^{-1} separates the high-frequency interband transitions from the low-energy excitations. The α - and β -infrared-active phonon modes are indicated in panel (c).

frequency for increasing temperature.³⁰ At variance with previous samples, the α mode in Bi_2Se_3 shows, instead, a high-frequency dip at all T 's, in agreement with the observation reported in Ref. 16. This behavior suggests that the electronic continuum is located, on average, at higher frequencies with respect to the α -phonon characteristic frequency.

In order to better follow the evolution of both the lattice and the electronic optical conductivities, we have fitted a D-L model to the $\sigma_1(\omega)$ model where the α -phonon mode is described in terms of the Fano shape.²⁹ Examples of those fits (dotted lines) are shown in the insets of Fig. 3, at 5 K.

The $\sigma_1(\omega)$ in the FIR region, as obtained after subtraction of both interband and phonon contributions, is shown in the main panels of the same figure. The electronic conductivity of Bi_2Se_3 [Fig. 3(a)] can be described in terms of a Drude term (open circles), which narrows for decreasing T in agreement with the metallic behavior of the resistivity¹⁸ and of a broad

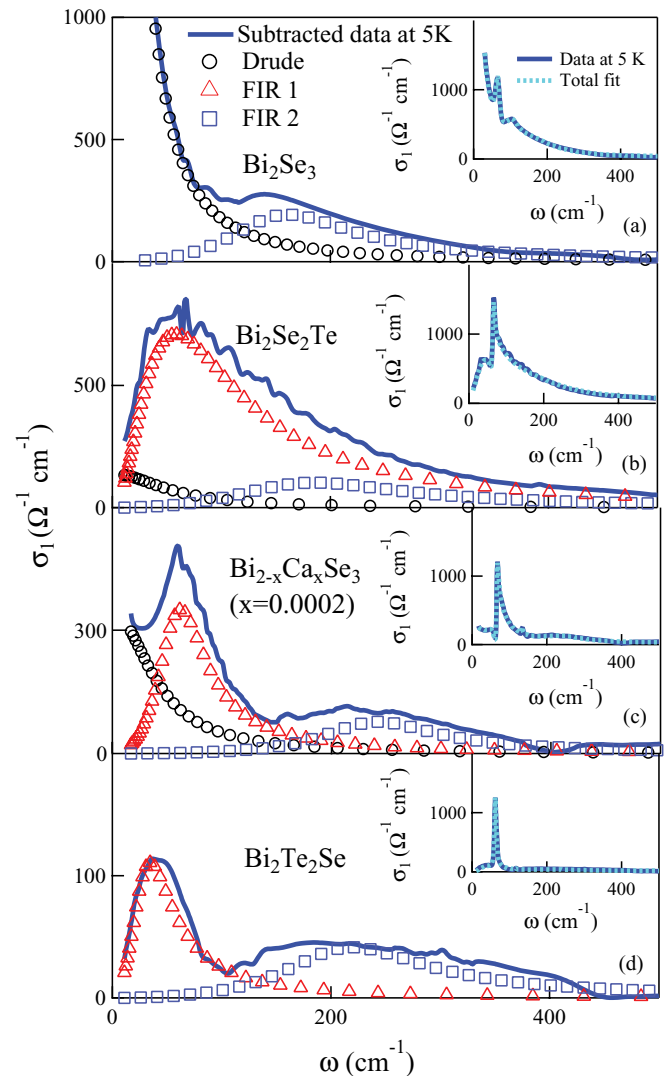


FIG. 3. (Color online) FIR optical conductivity at 5 K of the four Bi-based single crystals, after subtraction of both the interband and the phonon contributions *via* Drude-Lorentz fits. The Drude term and the FIR contributions 1 and 2 are indicated by open circles, triangles, and squares, respectively. Note the different vertical scales in each panel.

absorption centered around 150 cm^{-1} (open squares). In $\text{Bi}_2\text{Se}_2\text{Te}$ [Fig. 3(b)], most of the FIR spectral weight is located in a broad band centered around 100 cm^{-1} . This band has been modeled through two Lorentzian contributions, peaked around 50 cm^{-1} (open triangles, FIR1) and 200 cm^{-1} (open squares, FIR2). In $\text{Bi}_{1.9998}\text{Ca}_{0.0002}\text{Se}_3$, the increased compensation results in an overall reduction in the FIR spectral weight. Moreover, the FIR absorption, already observed in $\text{Bi}_2\text{Se}_2\text{Te}$ [Fig. 3(b)], splits into two bands: a narrow absorption centered at about 50 cm^{-1} and a broader one around 200 cm^{-1} . This double spectral structure is also achieved in $\text{Bi}_2\text{Te}_2\text{Se}$ where the low-frequency conductivity assumes a value comparable to the $\sigma_{dc} \sim 1 \text{ } \Omega^{-1} \text{ cm}^{-1}$ measured in crystals belonging to the same batch.²⁴

Similar low-frequency absorption bands have been observed in other more conventionally doped semiconductors, such as Si:P.^{31,32} Therein, an insulator-to-metal transition

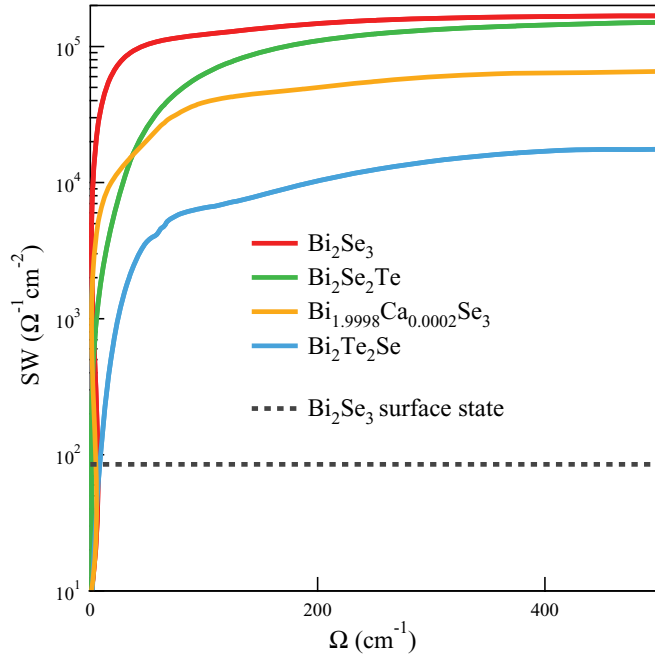


FIG. 4. (Color online) FIR spectral weight of all samples calculated at 5 K by Eq. (1). The dashed curve represents the contribution from the topological surface carriers as obtained from the data of Ref. 35.

(IMT) of Anderson type³³ can be observed for a charge-carrier density $n_{\text{IMT}} \sim 3.7 \times 10^{18}/\text{cm}^3$.^{31–33} Deep inside the insulating phase ($n < n_{\text{IMT}}$), narrow peaks can be observed in the FIR conductivity corresponding to the hydrogenlike $1s \rightarrow np$ transitions of isolated P impurities. They are followed by a broad band at higher frequencies due to the transitions from the impurity bound states to the continuum. The narrow peaks broaden for increasing doping, giving rise to a low-frequency band, which, however, remains distinguished from the higher-frequency absorption. When crossing the IMT, the low-frequency band transforms into a Drude term, while the high-frequency absorption persists in the metallic phase, indicating that the IMT occurs in an impurity band.³² Therefore, in analogy with Si:P, the FIR2 band at 200 cm^{-1} in $\text{Bi}_{1.9998}\text{Ca}_{0.0002}\text{Se}_3$ and $\text{Bi}_2\text{Te}_2\text{Se}$ can be assigned to the transitions from the impurity bound states to the electronic continuum. The FIR2 band is also in very good agreement with the impurity ionization energy estimated from the T dependence of resistivity and Hall data, namely, $E_i \sim 20\text{--}40 \text{ meV}$.^{23,24,34} Instead, the low-frequency FIR1 band, clearly resolved in both $\text{Bi}_{1.9998}\text{Ca}_{0.0002}\text{Se}_3$ and $\text{Bi}_2\text{Te}_2\text{Se}$ as shown in Figs. 3(c) and 3(d), respectively, can be associated with hydrogenlike $1s \rightarrow np$ transitions, broadened by the inhomogeneous environment of the impurities and/or

by their interactions. The spectra in Fig. 3 clearly show that, even in the most compensated topological insulator measured here, i.e., $\text{Bi}_2\text{Te}_2\text{Se}$, the FIR conductivity is still affected by extrinsic charge carriers due to nonstoichiometry and doping.

A more quantitative comparison between the charge density expected for the topological surface states and that provided by extrinsic charge carriers can be obtained by calculating the optical spectral weight $SW(\Omega)$,

$$SW(\Omega) = \int_0^\Omega \sigma_1^{\text{sub}}(\omega) d\omega, \quad (1)$$

where $\Omega = 500 \text{ cm}^{-1}$ is a cutoff frequency, which well separates (see Fig. 3) the low-frequency excitations from the interband transitions. In Fig. 4, one observes a decrease in the spectral weight by 1 order of magnitude from Bi_2Se_3 to $\text{Bi}_2\text{Te}_2\text{Se}$. This quantitatively shows the drastic effect of chemical compensation. From the previous SW , one can estimate a 3D charge density n for Bi_2Se_3 of about $3 \times 10^{18}/\text{cm}^3$, which becomes $\sim 10^{17}/\text{cm}^3$ for $\text{Bi}_2\text{Te}_2\text{Se}$. This value agrees very well with the range of $5 \times 10^{16}\text{--}2 \times 10^{17}/\text{cm}^3$ extracted from transport measurements in crystals of the same batch.²⁵

Recently, the THz conductivity of Bi_2Se_3 films grown by molecular-beam epitaxy has been measured by a time-domain technique from 200 GHz to about 2 THz.^{35,36} The optical conductivity in this spectral region can be satisfactorily fit by a two-dimensional (2D) Drude term plus the α -phonon mode. The 2D Drude contribution has been associated with topological surface states.^{35,36} Therefore, their spectral weight can be estimated from the Drude plasma frequency (ω_{SSP}) as obtained from the fit in Ref. 35: $SW_{SS} = \omega_{SSP}^2/8$. This value is plotted in Fig. 4 by the dashed line. The actual SW in $\text{Bi}_2\text{Te}_2\text{Se}$ is still higher, by nearly 2 orders of magnitude, than that expected from the topological surface states. This result indicates that the low-energy electrodynamics in single crystals of topological insulators, even at the highest degree of compensation presently achieved and at the lowest temperatures where infrared spectra are taken, is still influenced by 3D charge excitations. Therefore, further improvements in the compensation are needed before bulk techniques, such as infrared spectroscopy, may observe, in single crystals, the optical properties of purely topological metallic states.

ACKNOWLEDGMENTS

We acknowledge the Helmholtz-Zentrum Berlin-Electron storage ring BESSY II for provision of synchrotron radiation at beamline IRIS. The research leading to these results has received funding from the European Community's Seventh Framework Programme (FP7/2007-2013) under Grant Agreement No. 226716. The crystal growth was supported by the US National Science Foundation Grant No. DMR-0819860.

¹M. Z. Hasan and C. L. Kane, *Rev. Mod. Phys.* **82**, 3045 (2010).

²C. L. Kane and E. J. Mele, *Phys. Rev. Lett.* **95**, 226801 (2005).

³J. E. Moore, *Nature (London)* **464**, 194 (2010).

⁴L. Fu and C. L. Kane, *Phys. Rev. Lett.* **100**, 096407 (2008).

⁵A. R. Akhmerov, J. Nilsson, and C. W. J. Beenakker, *Phys. Rev. Lett.* **102**, 216404 (2009).

- ⁶X.-L. Qi, T. L. Hughes, and S.-C. Zhang, *Phys. Rev. B* **78**, 195424 (2008).
- ⁷A. M. Essin, J. E. Moore, and D. Vanderbilt, *Phys. Rev. Lett.* **102**, 146805 (2009).
- ⁸L. Fu and G. P. Collins, *Sci. Am.* **294**, 57 (2006).
- ⁹A. Kitaev and J. Preskill, *Phys. Rev. Lett.* **96**, 110404 (2006).
- ¹⁰X. Zhang, J. Wang, and S.-C. Zhang, *Phys. Rev. B* **82**, 245107 (2010).
- ¹¹Y. L. Chen, J. G. Analytis, J.-H. Chu, Z. K. Liu, S.-K. Mo, X. L. Qi, H. J. Zhang, D. H. Lu, X. Dai, Z. Fang, S. C. Zhang, I. R. Fisher, Z. Hussain, and Z.-X. Shen, *Science* **325**, 178 (2009).
- ¹²D. Hsieh, D. Qian, L. Wray, Y. Xia, Y. S. Hor, R. J. Cava, and M. Z. Hasan, *Nature (London)* **452**, 970 (2008).
- ¹³H. Zhang, C.-X. Liu, X.-L. Qi, X. Dai, Z. Fang, and S.-C. Zhang, *Nat. Phys.* **5**, 438 (2009).
- ¹⁴Y. Xia, D. Qian, D. Hsieh, L. Wray, A. Pal, H. Lin, A. Bansil, D. Grauer, Y. S. Hor, R. J. Cava, and M. Z. Hasan, *Nat. Phys.* **5**, 398 (2009).
- ¹⁵D.-X. Qu, Y. S. Hor, J. Xiong, R. J. Cava, and N. P. Ong, *Science* **329**, 821 (2010).
- ¹⁶A. D. LaForge, A. Frenzel, B. C. Pursley, T. Lin, X. Liu, J. Shi, and D. N. Basov, *Phys. Rev. B* **81**, 125120 (2010).
- ¹⁷N. P. Butch, K. Kirshenbaum, P. Syers, A. B. Sushkov, G. S. Jenkins, H. D. Drew, and J. Paglione, *Phys. Rev. B* **81**, 241301 (2010).
- ¹⁸Y. S. Hor, A. Richardella, P. Roushan, Y. Xia, J. G. Checkelsky, A. Yazdani, M. Z. Hasan, N. P. Ong, and R. J. Cava, *Phys. Rev. B* **79**, 195208 (2009).
- ¹⁹J. Black, E. M. Conwell, L. Seigle, and C. W. Spencer, *J. Phys. Chem. Solids* **2**, 240 (1957).
- ²⁰W. Richter and C. R. Becker, *Phys. Status Solidi B* **84**, 619 (1977).
- ²¹H. Zhang, C.-X. Liu, X.-L. Qi, X. Dai, Z. Fang, and S.-C. Zhang, *Nat. Phys.* **5**, 438 (2009).
- ²²G. A. Thomas, D. H. Rapkine, R. B. Van Dover, L. F. Mattheiss, W. A. Sunder, L. F. Schneemeyer, and J. V. Waszczak, *Phys. Rev. B* **46**, 1553 (1992).
- ²³Z. Ren, A. A. Taskin, S. Sasaki, K. Segawa, and Y. Ando, *Phys. Rev. B* **82**, 241306(R) (2010).
- ²⁴J. Xiong, A. C. Petersen, D. Qu, Y. S. Hor, R. J. Cava, and N. P. Ong, *Physica E* **44**, 920 (2012).
- ²⁵S. Jia, H. Ji, E. Climent-Pascual, M. K. Fuccillo, M. E. Charles, J. Xiong, N. P. Ong, and R. J. Cava, *Phys. Rev. B* **84**, 235206 (2011).
- ²⁶M. Abo-Bakr, J. Feikes, K. Holldack, P. Kuske, W. B. Peatman, U. Schade, G. Wüstefeld, and H.-W. Hübers, *Phys. Rev. Lett.* **90**, 094801 (2003).
- ²⁷D. L. Greenaway and G. Harbeke, *J. Phys. Chem. Solids* **26**, 1585 (1965).
- ²⁸R. J. Cava (private communication).
- ²⁹A. Damascelli, K. Schulte, D. van der Marel, and A. A. Menovsky, *Phys. Rev. B* **55**, R4863 (1997).
- ³⁰S. Lupi, M. Capizzi, P. Calvani, B. Ruzicka, P. Maselli, P. Dore, and A. Paolone, *Phys. Rev. B* **57**, 1248 (1998).
- ³¹G. A. Thomas, M. Capizzi, F. DeRosa, R. N. Bhatt, and T. M. Rice, *Phys. Rev. B* **23**, 5472 (1981).
- ³²A. Gaymann, H. P. Geserich, and H. v. Löhneysen, *Phys. Rev. B* **52**, 16486 (1995).
- ³³N. F. Mott, *Metal-Insulator Transitions* (Taylor and Francis, London, 1990).
- ³⁴Y. S. Kim, M. Brahlek, N. Bansal, E. Edrey, G. A. Kapilevich, K. Iida, M. Tanimura, Y. Horibe, S.-W. Cheong, and S. Oh, *Phys. Rev. B* **84**, 073109 (2011).
- ³⁵R. Valdés Aguilar, A. V. Stier, W. Liu, L. S. Bilbro, D. K. George, N. Bansal, L. Wu, J. Cerne, A. G. Markelz, S. Oh, and N. P. Armitage, *Phys. Rev. Lett.* **108**, 087403 (2012).
- ³⁶R. Valdés Aguilar, L. Wu, A. V. Stier, L. S. Bilbro, M. Brahlek, N. Bansal, S. Oh, and N. P. Armitage, [arXiv:1202.1249](https://arxiv.org/abs/1202.1249).